



Contribution of reaction of atmospheric amine with sulfuric acid to mixing particle formation from clay mineral



Weina Zhang^{a,b}, Zhenhao Guo^a, Weiping Zhang^{a,b}, Yuemeng Ji^{a,b}, Guiying Li^{a,b}, Taicheng An^{a,b,*}

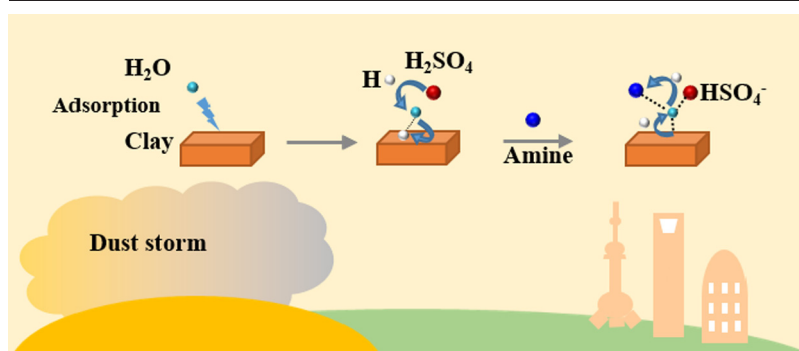
^a Guangdong-Hong Kong-Macao Joint Laboratory for Contaminants Exposure and Health, Guangdong Key Laboratory of Environmental Catalysis and Health Risk Control, Institute of Environmental Health and Pollution Control, Guangdong University of Technology, Guangzhou 510006, China

^b Guangzhou Key Laboratory of Environmental Catalysis and Pollution Control, Key Laboratory of City Cluster Environmental Safety and Green Development (Department of Education), School of Environmental Science and Engineering, Guangdong University of Technology, Guangzhou 510006, China

HIGHLIGHTS

- Atmospheric amines contribute to mixing particle formation during dust storm.
- MA and DMA contribute more to mixing particle formation than TMA.
- Protonated mineral surface is key intermediate during mixing particle formation.
- Water content is requirement for mixing particle formation from MA.

GRAPHICAL ABSTRACT



ARTICLE INFO

Article history:

Received 29 November 2021

Received in revised form 26 December 2021

Accepted 18 January 2022

Available online 22 January 2022

Editor: Jianmin Chen

Keywords:

Atmospheric amines

Sulfuric acid

Water

Clay mineral

Mixing particle formation mechanism

ABSTRACT

During dust storm, mineral particle is frequently observed to be mixed with anthropogenic pollutants (APs) and forms mixing particle which arises more complex influences on regional climate than unmixed mineral particle. Even though mixing particle formation mechanism received significant attention recently, most studies focused on the heterogeneous reaction of inorganic APs on single composition of mineral. Here, the heterogeneous reaction mechanism of amine (a proxy of organic APs) with sulfuric acid (SA) on kaolinite (Kao, a proxy of mineral dust), and its contribution to mixing particle formation are investigated under variable atmospheric conditions. Two heterogeneous reactions of Kao-SA-amine and Kao-H₂O-SA-amine in absence/presence of water were comparably investigated using combined theoretical and experimental methods, respectively. The contribution from such two heterogeneous reactions to mixing particle formation was evaluated, respectively, exploring the effect of methyl groups (1–3 -CH₃), relative humidity (RH) (11–100%) and temperature (220–298.15 K). Water was observed to play a significant role in promoting heterogeneous reaction of amines with SA on Kao surface, reducing formation energy of mixing particle containing ammonium salt converted by SA. Moreover, the promotion effect from water is enhanced with the increasing RH and the decreasing temperature. For methylamine and dimethylamine containing 1–2 -CH₃, the heterogeneous reaction of Kao-H₂O-SA-amine contributes more to mixing particle formation. However, for trimethylamine containing 3 -CH₃, the heterogeneous reaction of Kao-SA-amine is the dominant source to mixing particle formation. For mixing particle generated from the above two heterogeneous reactions, ammonium salts are supposed to be predominant components which is of strong hygroscopicity and further leads to significant influence on climate by altering radiative forcing of mixed particle and participating in the cloud condensation nuclei and ice nuclei.

* Corresponding author at: Guangdong-Hong Kong-Macao Joint Laboratory for Contaminants Exposure and Health, Guangdong Key Laboratory of Environmental Catalysis and Health Risk Control, Institute of Environmental Health and Pollution Control, Guangdong University of Technology, Guangzhou 510006, China.

E-mail address: antc99@gdut.edu.cn (T. An).

1. Introduction

Mineral dusts contribute the most by mass to atmospheric aerosol (Kok et al., 2017). An estimated emission amount of 1000–3000 Tg yr⁻¹ of mineral dusts are released to atmosphere (Yu and Jang, 2018), leading to significant influence on climate by radiative forcing and participating in the cloud condensation nuclei (CCN) and ice nuclei (IN) (DeMott et al., 2010; Zhang et al., 2020). Massive mineral dusts are transported over several kilometers. For instance, dust could be transported from the inner Asian continent to the Pacific and even to the North America by passing over China (Zhou et al., 2018). During their life time of long transport, mineral dusts are found to form mixing particles with many anthropogenic pollutants (APs) (Burgos et al., 2016), such as organics, as well as inorganics including nitrogen and sulfur, variable salt-containing aerosols and ozone (Du et al., 2019; Gong et al., 2021; Tan et al., 2017), through heterogeneous uptakes and chemical reactions in urban regions. During these processes, mineral dust is found to significantly affect heterogeneous reaction mechanisms of APs and lead to further components changes of particle (Ponczek and George, 2018; Wang et al., 2018). Previous experimental studies also revealed that mixing particles exhibit significantly enhanced absorbing ability than the corresponding unmixed dust and anthropogenic aerosols (Tian et al., 2018).

Recently, the mixing particle formation mechanisms (Ryder et al., 2014; Tian et al., 2018; Wang et al., 2018) have received many attractions. In these investigations, single composition of mineral dusts, such as Al₂O₃ (Yang et al., 2020; Yang et al., 2019), SiO₂ (Ji et al., 2015) TiO₂ (Chen et al., 2021) and iron oxide (Kadar et al., 2014; Moteki et al., 2017) are popularly explored, and all the investigations declare the compositions and structures of these mineral dust surfaces significantly affect the gaseous AP uptake by mineral dust and subsequent heterogeneous reactions of APs, determining the final chemical composition and the ability of mixing particle to affect atmospheric environment. Clay mineral, a complex-component mineral, is rarely attempted although it contributes most to mineral dust. Especially, clay mineral is composed of layered silicates and aluminates, leading to its strong hydrophilicity, and water uptake easily proceeds on its surface (Tenney and Cygan, 2014). Previous experimental results noted that monolayer water can be developed on clay mineral surface even at very dry condition (11% relative humidity, 11% RH) (Gustafsson et al., 2005). Other experiment further proved that the evaporation of water leaves OH groups on clay mineral dust (Ponczek and George, 2018), and the hydroxylated surface subsequently affects the heterogeneous uptake and reaction processes of APs (Cuadros et al., 2015; Herich et al., 2009). Therefore, the detailed influences of wide RH range observed in the troposphere on the mixing particle formation from clay mineral should be investigated. Besides, RH temperature is another important factor that affects particle formation mechanism.

Amine is a typical alkaline volatile organic compound which is common in secondary organic aerosol (Tong et al., 2020). Recently, amine has attracted lots of attentions because of its stronger ability in accelerating new particle formation (Shen et al., 2020; Xie et al., 2017). For example, ppt. Level of dimethylamine (DMA) in atmospheric environment was found to enhance the formation rates of particle through ammonium salt conversion obtained from the reaction of sulfuric acid (SA) more than 1000-fold compared with ammonia (Almeida et al., 2013). Recent studies further observed SA-DMA cluster formations in megacities of China (Yao et al., 2018). The other two classical types of light-weight-mass amines, namely methylamine (MA) and trimethylamine (TMA), also deserve attractions due to their abundance compared to the other amines in the atmosphere (Ge et al., 2011) and their contributions to new particle formation (NPF) through forming SA-amine clusters (VandenBoer et al., 2011).

However, up to now, little work is attempted to explore the contributions of these amines to the mixing particle formation although it has been observed in Pearl River Delta, China (Cheng et al., 2018). Hence, in this work, typical light mass weighted amines, namely MA, DMA and TMA, are selected as the proxy of VOCs (Julin et al., 2018; Zhang et al., 2019) to study the mixing particle formation from kaolinite (Kao), the most commonly employed clay mineral. To further assess the effect of

water on the mixing particle formation, two systems of Kao-SA-amine and Kao-H₂O-SA-amine in absence/presence of water are comparably investigated, respectively. Amine type, as well as wide RH and temperature ranges, is considered to investigate their influences on the mixing particle formation mechanisms. The uptakes of amines as well as H₂O and SA, were firstly simulated by classical molecular dynamics (MD), and the formation mechanisms were subsequently calculated by density function theory (DFT). Zeta potential measurements was carried out to verify the stability of key intermediate during mixing particle formations.

2. Methods

2.1. Theoretical simulations

Considering lower concentration of atmospheric amines than water and SA vapors, the heterogeneous uptakes of single SA and H₂O molecules are first simulated on the (001) surface containing AlO sheet of Kao using classical MD method. All the classical MD simulations are performed using the package of Nanoscale Molecular Dynamics (Phillips et al., 2005). The free energy profile is then calculated combining umbrella methods and weighted histogram analysis method (Kumar et al., 1995) based on all trajectories obtained from classical MD simulations. The uptake sites of single SA and H₂O molecule on Kao surface (Fig. S1) are separately determined by the most stable configurations with the lowest free energy along their uptake paths, respectively.

Each type of amine is subsequently introduced to the most stable structures of Kao-SA and Kao-H₂O, respectively. The interactions between amine and Kao surface are analyzed by radial distribution function (RDF) which describes a kind of atom A distribution centered on another kind of atom B. The horizontal and vertical coordinates represent distance between two atoms and the occurrence probability of atom A, and narrow and high peaks indicate strong interactions between atoms A and B. To further confirm the mixing particle formation mechanisms of the two systems of Kao-SA-amine and Kao-H₂O-SA-amine, the formation energies (ΔE) of all intermediates and products along each plausible formation path are calculated using DFT calculations performed by package of Vienna ab initio simulation package (VASP) (Kresse and Furthmüller, 1996). For the convenience of comparisons, all values of ΔE for the two systems are determined based on Kao surface (0 kcal/mol). More simulation details of MD and DFT, as well as the kinetic calculations are all provided in Supplementary data.

Finally, to quantitatively compare the contributions of the above two mechanisms to the mixing particles under the tropospheric conditions, the final product ratio (γ) is defined as [amineH⁺·HSO₄⁻·H₂O·Kao]/[amineH⁺·HSO₄⁻·Kao], and calculated at variable RH and temperatures. The detailed derivation is also provided in Supporting information (SI).

2.2. Zeta potential measurements

To clarify the stability changes of Kao after water and SA uptakes, zeta potentials of Kao with water and SA-water vapors are measured. Four samples, namely i) pure Kao particle (Kao), ii) Kao with pure water vapor (Kao-H₂O), iii) Kao with 10 vol% (volume fraction) of SA vapor (Kao-10% SA) and iv) Kao with 50 vol% of SA solution vapor, are prepared using a bubbling method (gas flow rate: 30 mL/min; adsorption time: 2 h). 0.1 wt% (0.001 g/mL) of the four samples is separately suspended in ethyl alcohol and sonicated in an ultrasonic bath for 10 min to achieve consistent dispersion of particles. Zeta potential distribution (Figs. S2 – S5) is measured using a Nano-Zetasizer (Malvern Instruments, Zetasizer Nano S90, UK). Measurement of each sample is repeated three times, and the final zeta potential values are determined by related average values with error bars.

3. Results and discussion

3.1. Heterogeneous uptakes of SA and water by the Kao surface

Free energy profile is commonly used to describe the thermodynamic feasibility of uptake and predicate the uptake sites of trace gas

(Li et al., 2021; Zhang et al., 2019). Fig. 1A depicts the free energy profiles of single SA and H₂O molecules during the heterogeneous uptake processes to Kao surface, respectively, obtained from MD simulations. $Z = 0$ indicates the position of the exposed Kao surface. For water uptake by Kao surface, the free energy value dramatically decreases from $Z = 9.4 \text{ \AA}$, indicating thermodynamic feasibility. Meanwhile, the minimum free energy of water exists at $Z = 1.9 \text{ \AA}$, implying the uptake site of water locates at very close to Kao surface. As for the SA uptake by Kao surface, the initial decreasing tendency of free energy also explains the SA uptake to Kao surface is feasible in thermodynamic, which is similar to water uptake. However, the uptake site of SA locates at a farther position ($Z = 3.2 \text{ \AA}$) than that of H₂O ($Z = 1.9 \text{ \AA}$) due to larger molecule size of SA than H₂O. Hence, in terms of competition of SA with H₂O from the perspective of steric hindrance, the size of H₂O molecule is smaller, giving it advantage to react first with Kao surface. Therefore, mixing particle formation starting from water uptake as the first step is plausible.

Besides the uptake site position, the accumulated concentration of SA and water on Kao surface also determines the first step of mixing particle formation. According to our previous work (Zhang et al., 2021), the concentration profiles of trace gases can be calculated by the equation of $c(Z) = e^{-\Delta E/RT} c_{\text{gas}}$, where ΔE represents the free energy difference between arbitrary Z to Kao surface ($Z = 0$), c_{gas} represents atmospheric concentration of trace gases (SA and water in this work), and R and T represent ideal gas constant and temperature, respectively. The average concentration of SA vapor in the atmosphere is typically in the range of 10^5 – 10^7 molecules cm^{-3} (Erupe et al., 2010). Thus, the calculated concentration of SA on Kao surface is $4.011 \times 10^{12-14}$ molecules cm^{-3} . Meanwhile, based on experimental results (Gustafsson et al., 2005), our model of Kao-H₂O corresponding to monolayer water flat on Kao surface is proposed at 11% RH. Accordingly, the concentration of water vapor in the atmosphere is estimated to be 10^{16} molecules cm^{-3} . Thus, the accumulated concentration of water on Kao surface, namely the highest concentration value in Fig. 1B, is 1.09×10^{20} molecules cm^{-3} , which is 5–7 orders higher than that of SA to the Kao surface. The accumulated concentration of water on Kao surface increases in portion to RH values. The much higher concentration of accumulated water on Kao surface than that of SA furthermore profoundly increases the probability of mixing particle formation starting from water uptake even at very dry condition (11% RH).

3.2. Key intermediates formed in the presence/absence of water

Following uptakes of SA and water, the clusters of KaoSA and KaoH₂O are subsequently formed (Fig. S6). Next, the formation mechanisms of the two cluster are comparably investigated. For KaoSA cluster, it is observed to be formed through a spontaneous protonation of Kao surface by SA, existing as $\text{HSO}_4^- \cdot \text{KaoH}^+$ with negative ΔE of -29.85 kcal/mol (Fig. S6A). Three alkaline amines studied in this work are also easily protonated by SA, which acts as a critical process in NPF (Almeida et al.,

2013; Yin et al., 2021). To our best knowledge, the calculated ΔE of SA·MA, SA·DMA and SA·TMA clusters are reported to be approximately -10 – -20 (Lv et al., 2015), -11 – -17 (Nadykto et al., 2014; Olenius et al., 2013) and -16 kcal/mol (Olenius et al., 2017), respectively, at relevant atmospheric conditions. Significant differences in the reported ΔE of these SA-amine clusters are accounted for different calculated levels of theory. Nevertheless, the ΔE of KaoSA cluster (-29.85 kcal/mol) is much lower than that of any SA-amine cluster, implying KaoSA cluster is more stable than SA-amine clusters and Kao could compete with amines to react with SA. It is reasonably speculated that mixing particle formation would contribute to NPF during dust storm carrying massive clay minerals. This could partially explain why massive mixing particles containing sulfate salts are observed after dust storm (Song et al., 2012). Moreover, $\text{HSO}_4^- \cdot \text{KaoH}^+$ derived from KaoSA cluster has one hydrogen bonding site that is sterically available for further addition of amine or other species (Fig. S6A). Therefore, without water, KaoSA cluster should be treated as the key intermediate to furthermore react with amines to form mixing particle.

Different from the formation mechanism of KaoSA cluster, KaoH₂O cluster is formed through hydrogen bonds of H₂O molecule with Kao surface and produces H₂O-Kao complex (Fig. S6B), which gives straightforward evidence to the speculation of a previous experiment (Ponczek and George, 2018). The corresponding ΔE of KaoH₂O cluster (-11.97 kcal/mol) is higher than that of KaoSA cluster (-29.85 kcal/mol), indicating lower stability of KaoH₂O than KaoSA cluster. Therefore, acid precursor, such as SA, is necessary to be induced into KaoH₂O cluster to form more stable intermediate to compete with KaoSA cluster.

As expected, KaoH₂O-SA cluster (Fig. S6C) exhibits higher stability than KaoH₂O cluster due to the addition of SA, which is proved by lower ΔE of KaoH₂O-SA cluster (-42.30 kcal/mol) than that of KaoH₂O cluster (-11.97 kcal/mol). $\text{HSO}_4^- \cdot \text{H}_2\text{O} \cdot \text{KaoH}^+$ is spontaneously produced through a reaction of double-proton transfer, namely proton c of SA is transferred to H₂O and simultaneously proton d of H₂O is transferred to Kao surface (Fig. S6C). Meanwhile, the zeta potential values of Kao-10% SA and 50% SA are both found to be higher than those of KaoH₂O cluster and Kao particle (Fig. 2), proving that KaoH₂O-SA cluster is indeed more stable than original KaoH₂O cluster. More importantly, the water addition brings two more hydrogen bonding sites for the KaoH₂O-SA cluster than KaoSA cluster, and decreases ΔE of KaoH₂O-SA cluster than that of KaoSA cluster (Fig. S6A and S6C). Such benefits from water allows more amine additions from gas phase, eventually forming mixing particle. This character of water has also been shown in cluster formation in gas (Dawson et al., 2012). In conclusion, in the presence of water, KaoH₂O-SA cluster should be regarded as another intermediate that could be competitive with KaoSA intermediate in reacting with amines to form mixing particle. This furthermore reveals SA acts as the key precursor in the initial stage of mixing particle formation, which is similar to that in nucleation of vapors (Sipila et al., 2010; Zhang et al., 2004).

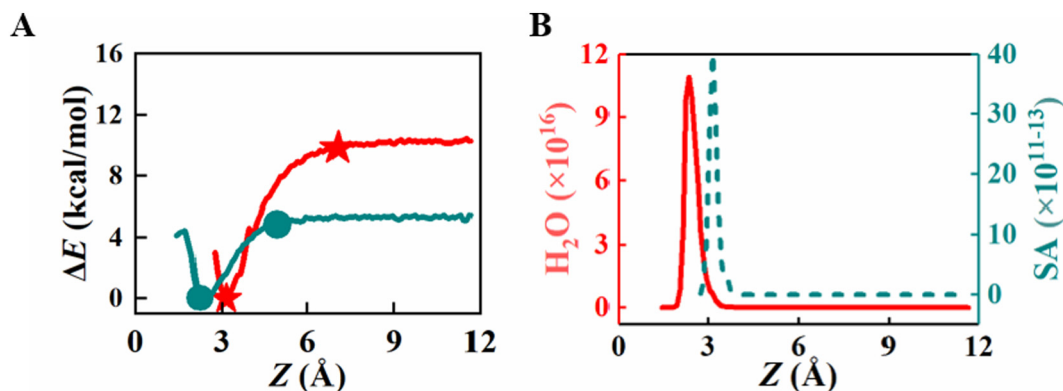


Fig. 1. (A) Free energy (E) profiles of single SA (red line) and H₂O (green line) molecules approaching Kao surface from gas phase, respectively. (B) Concentration profiles of SA (red line) and H₂O (green line) vapors along their heterogeneous uptake paths. $Z = 0$ represents the position of Kao surface.

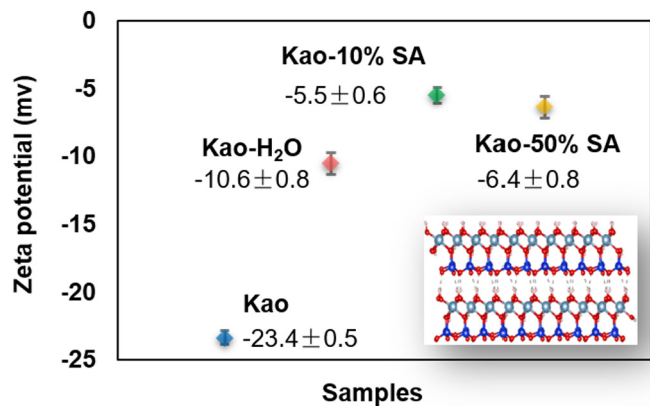


Fig. 2. Zeta potentials of variable Sample. Kao, Kao-H₂O, Kao-10% SA and Kao-50% SA are referred to blue, red, green and yellow squares. The corresponding zeta potential values are displayed below each sample name.

Considering two different intermediates formed in the presence/absence of water, the formation mechanisms of Kao-SA-amine and Kao-H₂O-SA-amine systems are comparably analyzed below.

3.3. The mixing particle formation mechanisms of Kao-SA-amine system

Concentration is first focused on Kao-SA-amine system. To illustrate the changes in active site distribution arised from amine uptake by Kao-SA cluster, the active sites of SA reacting with the Kao surface before and after uptakes of three amines are compared using RDFs as displayed

in Fig. 3. Potential active sites of SA or amines reacting with Kao surface are predicted by narrow and high peaks of RDF.

Before amine uptake, the potential active sites of Kao-SA cluster are illustrated in Fig. 3A. Within SA molecule, potential active site on hydrogen atoms is denoted by H(SA), and the other two potential active sites on oxygen atoms, bonding with sulfate atom through SO and SO bonds, are represented by O2(SA) and OR(SA), respectively. As for Kao surface, active sites on oxygen and hydrogen atoms of OH group are separately represented by symbols of oh and ho. Fig. 3A displays that H(SA) is more active than O2(SA) while SA combines with Kao surface before the uptake of amines, marked by stronger signals of H(SA)-oh RDF than O2(SA)-ho RDF, indicating new bond formation between H(SA) and oh on Kao surface. This is consistent with the yield of HSO₄⁻·KaoH⁺ intermediate (Fig. S6A).

Following SA uptake, three amines are separately added onto Kao-SA cluster. First in the system of Kao-SA-MA, the active site distribution of SA reacting with Kao surface is displayed by RDFs as shown in Fig. 3B. The results explain active sites are of SA focused on H(SA) and O(SA) marked by strong signals of RDFs for H(SA)-oh and O2(SA)-ho, implying SA still keeps binding with Kao surface through two HO hydrogen bonds after MA addition. The active site distribution of MA reacting with Kao surface is also analyzed by RDF in Fig. S7A, where NR denotes active site on N of amine, and HNR and HCMM represent active sites on H atoms binding with N and C of amine, respectively. Unexpectedly, no obvious signal is observed on any RDF of MA, indicating MA exhibits weaker proton affinity to SA than Kao surface without water. The optimized structure of Kao-SA-MA cluster by DFT (right corner in Fig. 3B) further confirms that MA is unprotonated and Kao surface keeps protonated as KaoH⁺ after MA addition, yielding a more stable product of MA·HSO₄⁻·KaoH⁺ than HSO₄⁻·KaoH⁺. The observation of unprotonated MA implies that MA shows weaker alkalinity than Kao surface, and the ammonium salt conversion of

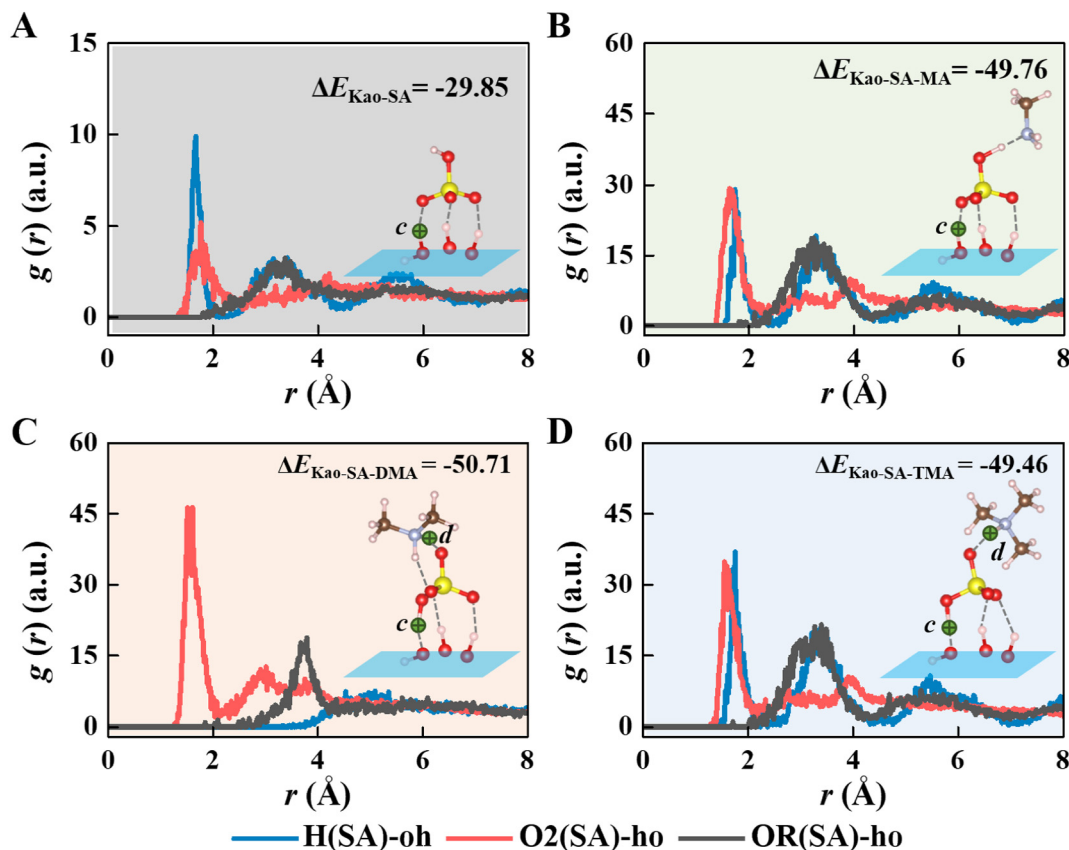


Fig. 3. RDFs of SA reacting with Kao surface within corresponding clusters of (A) Kao-SA, (B) Kao-SA-MA, (C) Kao-SA-DMA and (D) Kao-SA-TMA, respectively. ΔE (unit: kcal/mol) represents corresponding formation energy of the clusters, baed on Kao surface, obtained by DFT calculations. The definitions of symbols in the corner figures: Dashed line represents hydrogen bonds, and blue plane represent Kao surface. Colour code: red, oxygen atom; pink, hydrogen atom; yellow, sulfur atom; blue, nitrogen atom; brown, carbon atom, green with cross, transferred proton.

MA by SA is hereby unfavorable on Kao surface without water. This is completely different from the cluster formation of MA-SA in gas phase or liquid aerosol, where MA is easily converted into less volatile ammonium salts (Lv et al., 2015; Zhang et al., 2019; Zhang et al., 2021). Since unprotonated MA keeps higher volatile than its relevant ammonium salt, MA tends to escape from the Kao surface and contributes little to mixing particle formation in the absence of water.

By contrast to MA, Fig. 3C and D separately depicts the active site distributions of Kao-SA cluster after the additions of DMA and TMA. Similar to that in the system of Kao-SA-MA, SA keeps binding with Kao surface after addition of DMA or TMA, which is indicated by two obvious peaks of RDFs of H(SA)-oh and O2(SA)-ho. However, different from MA, DMA and TMA show stronger proton affinity to SA when reacting with Kao-SA intermediate, which is proved by obvious peaks of corresponding NR-ho RDFs (Fig. S7B and S7C). The optimized structures of Kao-SA-DMA and Kao-SA-TMA further confirm final products of DMAH⁺·HSO₄⁻·Kao and TMAH⁺·HSO₄⁻·Kao are spontaneously generated through a double-proton transfer reaction: SA recaptures proton *c* from Kao surface, and the nitrogen atoms of DMA or TMA simultaneously takes proton *d* from SA. The corresponding ΔE of DMAH⁺·HSO₄⁻·Kao and TMAH⁺·HSO₄⁻·Kao complexes are obtained as 20.86 and 19.61 kcal/mol lower than that of HSO₄⁻·Kao intermediate, implying the conversion of the two complexes exhibit thermodynamical feasibility. Interestingly, the addition of DMA or TMA to Kao-SA induces conversion of KaoH⁺ back to Kao, and both DMA and TMA are hereby protonated as ammonium salts. The results suggest DMA and TMA are more alkaline than Kao surface, leaving the traditional acid-base mechanism proposal in the mixing particle formation without water. Therefore, completely different from MA, DMA and TMA can efficiently contribute to mixing particle mass through ammonium salt conversion without water.

3.4. The mixing particle formation mechanisms of Kao-H₂O-SA-amine system

Next, the mixing particle formation mechanism of the Kao-H₂O-SA-amine system is explored. Besides hydrogen site (H-site) of HSO₄⁻ (H1), the Kao-H₂O-SA intermediate has two more H-sites (H2 and H3) due to the presence of water (Fig. 4A). Accordingly, for each amine, three possible formation pathways are considered when each amine is added at H1, H2 and H3-sites.

First, all the structures and related ΔE of all possible products formed in Kao-H₂O-SA-MA system are shown in Fig. 4B. ΔE of the three clusters for MA bonded to H1, H2 and H3-sites, respectively, are found to be 17.38, 20.56 and 15.62 kcal/mol lower than that of the Kao-H₂O-SA intermediate, implying all reactions proceeding are thermodynamically feasible. The corresponding final products for MA bonded to H1, H3-sites are both MA·HSO₄⁻·H₂O·KaoH⁺, and the product formed at H2-site is MAH⁺·SO₄²⁻·H₂O·KaoH⁺. Hence, the protonation of MA is only plausible at H2-site belonging to H₂O molecule, although H1 belongs to the same H₂O molecule as H2. To further elucidate why the different conversions of MA occurs at H2 and H3-sites, the charge density difference (CDD) for the Kao-H₂O-SA intermediate is additionally analyzed in Fig. S8. The CDD results illustrates that H2 is attracted by O(SA), whereas H3 is just bonded with O of H₂O. Thus, O(SA) drives H2 to be off O of H₂O, leading to covalent bond formation of H2 with N of amine instead of hydrogen bond formation with N of amine. Hence, at H2-site, the presence of water could promote ammonium salt conversion of MA and increase mass growth of mixing particle, which is not observed in the mixing particle formation without water. It is speculated water is necessary for MA to form mixing particle with Kao, whereas it is not for MA to form cluster with SA in vapor phase (Lv et al., 2015).

Similar to that in the MA system, DMA and TMA are also merely protonated at H2-site and keep unprotonated at the other two H-sites in the Kao-H₂O-SA-DMA and Kao-H₂O-SA-TMA systems as shown in Fig. 4C and D. However, different from MA, water is unnecessary for DMA and TMA to achieve ammonium salt conversion because DMAH⁺ and TMAH⁺ are readily produced in the mixing particle formed in the absence of water as mentioned above.

Note that ΔE of the TMAH⁺·HSO₄⁻·H₂O·Kao (-56.23 kcal/mol) at H2-site is much higher than those for MAH⁺·HSO₄⁻·H₂O·Kao and DMAH⁺·HSO₄⁻·H₂O·Kao (-62.86 and -65.03 kcal/mol), implying the product for TMA is less stable than MA and DMA formed at H2-site. Previous experiment of Liu et al. found that the steric effect of amines governs the reactivity of amines to form salts (Liu et al., 2012). Accordingly, the less stability of the structures for TMA is partially attributed to the larger steric hindrance of TMA because of its more methyl groups than MA and DMA. Additionally, as illustrated in Fig. S9A and S9B, both MAH⁺ and DMAH⁺ strongly interact with Kao surface though atom pair of HNR-oh, which is confirmed by obvious peaks (blue lines). However, in the product for TMA, no obvious peaks are observed on any RDF curve, indicating that TMAH⁺ barely interacts with Kao surface (Fig. S9C). Therefore, the less stability for the structure containing TMA is also resulted from the weaker interactions of TMAH⁺ than those of MAH⁺ and DMAH⁺ with Kao surface. As a result, the presence of water increases the stability of the mixing particle containing MA and DMA salts. This further suggests MA and DMA salts would contribute more to mixing particle compared to TMA salt in the presence of water.

3.5. RH and temperature effects on the final product generations

Based on the above results, Fig. 5A summarizes the corresponding schemes of the mixing particle containing ammonium salts. The related ΔE changes along the two pathways are comparably displayed in Fig. 5B and C. To quantitatively compare the contributions of the two mechanisms to the mixing particles at variable RH values and temperatures, the final product ratio (γ) is defined as [amineH⁺·HSO₄⁻·H₂O·Kao]/[amineH⁺·HSO₄⁻·Kao], which is referred to Ji et al.'s work (Ji et al., 2015). As described in 1.4 section of SI, γ can be determined as $\frac{K_3 \cdot K_4 \cdot K_5}{K_1 \cdot K_2} [\text{H}_2\text{O}]$, where K_i corresponds to equilibrium constants as labelled in Fig. 5A, and [H₂O] presents the observed concentration of water vapor at a given value of RH. Fig. 6 depicts γ changes for the three amines' cases at variable RH values and temperatures (T). Since MA salt formation is unfeasible without water, [MA·HSO₄⁻·KaoH⁺] is instead of [MAH⁺·HSO₄⁻·Kao] to calculate γ for MA case.

For mixing particle formation from the three amines, the RH effect on γ is first explored at condition of RH = 10% – 100% and T = 298.15 K. For MA case, as displayed in Fig. 6A, γ for MA shows remarkably correlated linearly with RH, which increases from 1.14×10^2 to 1.14×10^3 with the rising RH from 10 to 100%. The results imply the concentration of mixing particle composed of MAH⁺·HSO₄⁻·H₂O·Kao keeps 2–3 orders larger than that composed of MA·HSO₄⁻·KaoH⁺. The temperature effect on γ is next explored at condition of T = 220–298.15 K and RH = 11%. T range of 220–298.15 K is chosen according to T profile along altitudes of 0–12 km within the troposphere (Ji et al., 2015). Contrary to that with the rising RH, as shown in Fig. 6B, γ for MA presents downward trend with the increasing T , and is at least 73.7. This indicates the concentration of mixing particle composed of MAH⁺·HSO₄⁻·H₂O·Kao is at least 73.7 times the concentration of that involved MA·HSO₄⁻·KaoH⁺. Similar to γ profiles for MA case, γ for DMA increases with RH but decreases with T as displayed in Fig. 6C and D. More importantly, γ for DMA is also much larger than 1.0, indicating the concentration of mixing particle composed of DMAH⁺·HSO₄⁻·H₂O·Kao is estimated to be larger than that towards DMA·HSO₄⁻·KaoH⁺. Therefore, for the mixing particle formation close to MA or DMA source, MAH⁺·HSO₄⁻·H₂O·Kao or DMAH⁺·HSO₄⁻·H₂O·Kao is supposed to be the major component in the mixing particle, and the formation mechanism from water addition is dominant. At this point, water profoundly affects mixing particle formation from MA and DMA sources. The water content would benefit subsequent mixing particle growth through providing more hydrogen bonding sites, which is commonly confirmed in atmospheric reactions by other theoretical work (Dawson et al., 2012; Zhang et al., 2021).

γ for TMA case also shows positive correlation with the RH and negative correlation with T (Fig. 6C and D). However, γ for TMA case is always below 1.0 at any condition of RH and T . For instance, at

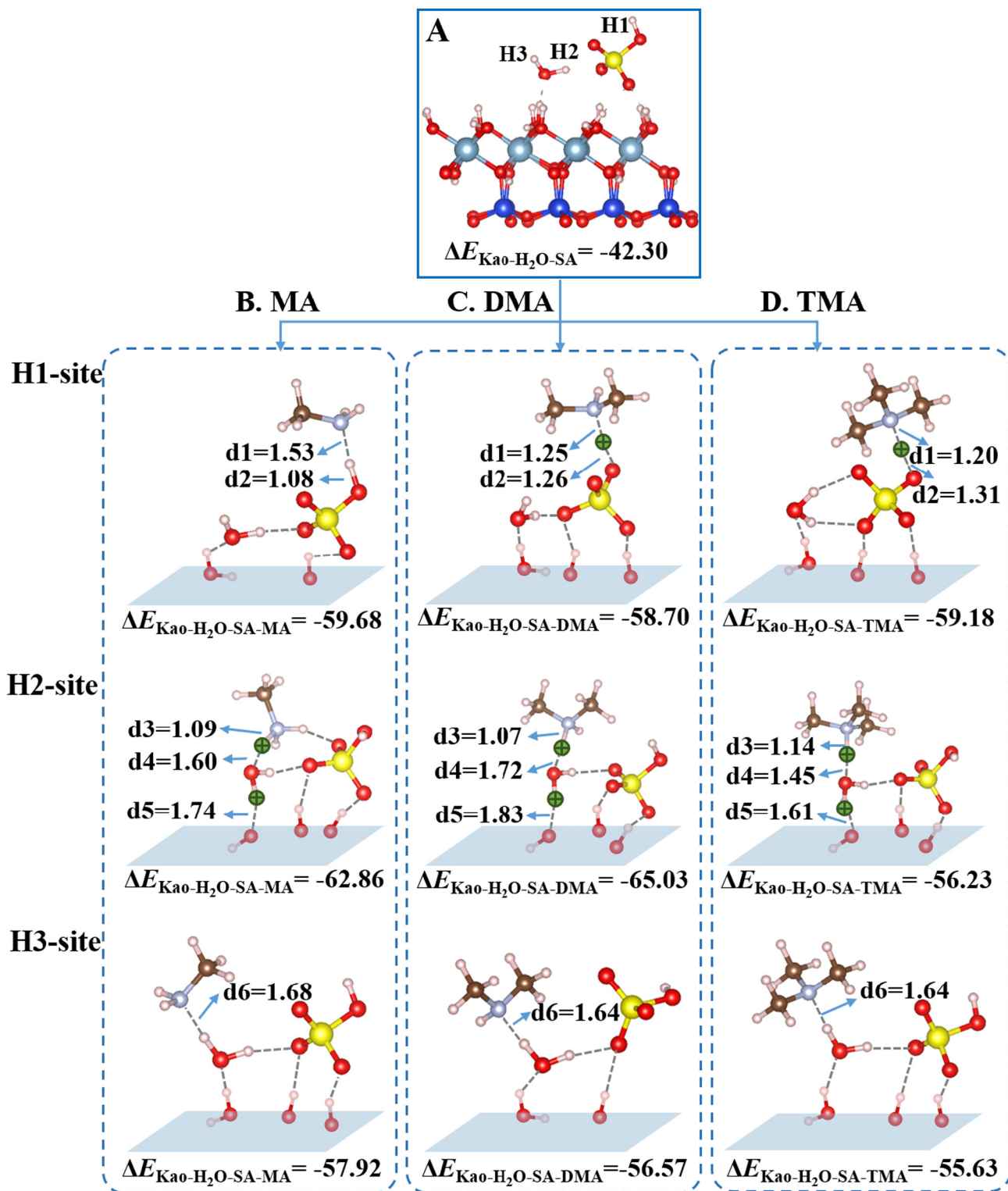


Fig. 4. (A) Mixing particle of Kao-H₂O-SA. Mixing particles containing (B) MA, (C) DMA and (D) TMA. The first, middle and final rows represent each amine is induced at H1, H2 and H3-sites, respectively. All the optimized mixing structures and corresponding formation energies (ΔE , in unit of kcal/mol), based on Kao surface, are obtained by DFT calculations. The colour codes are the same as those in Fig. 3. Bond length: Å in unit.

condition of RH = 10% – 100% and $T = 298.15$ K, γ decreases from 0.13 to 0.013 far below 1.0. Such range of γ indicates the concentration of mixing particle composed of $\text{TMAH}^+ \cdot \text{HSO}_4^- \cdot \text{H}_2\text{O} \cdot \text{Kao}$ is only 1.3% – 13% of that composed of $\text{TMAH}^+ \cdot \text{HSO}_4^- \cdot \text{Kao}$. The smaller concentration of $\text{TMAH}^+ \cdot \text{HSO}_4^- \cdot \text{H}_2\text{O} \cdot \text{Kao}$ can be explained by its low stability as mentioned above. Therefore, contrary to MA and DMA cases, water

addition has little effect on the mixing particle formation from TMA source. For mixing particle formation close to TMA source, the formation mechanism without water is the major one, and primary component is predicted to be $\text{TMAH}^+ \cdot \text{HSO}_4^- \cdot \text{Kao}$.

Overall, each amine is proved to contribute to mixing particle formation through ammonium salt conversion in wide ranges of RH and temperature

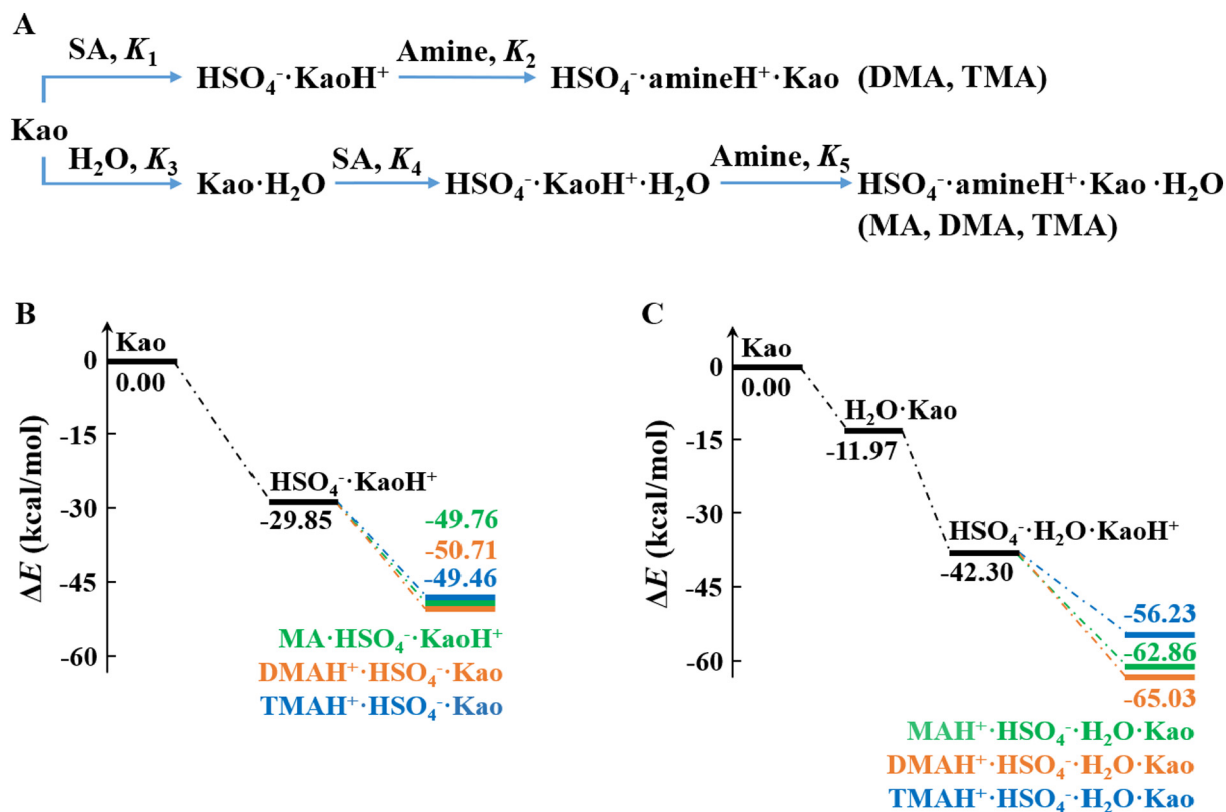


Fig. 5. (A) Proposed formation schemes for mixing particles. Formation energy changes along all mixing particle formation paths (B) in the absence and (C) presence of water. K_i represents corresponding equilibrium constants.

in the troposphere. Many megacities of China, such as Beijing, Nanjing, Shanghai, and Guangzhou, have adequate anthropic emissions of amines (Ge et al., 2011). Recently, SA-amine cluster was observed during NPF in Beijing and Shanghai (Yao et al., 2018; Yin et al., 2021). Dust aerosol contributes most by mass to atmospheric particle, and an estimated emission amount of 1000–3000 Tg yr⁻¹ of mineral dusts are released to atmosphere (Yu and Jang, 2018). Massive dust aerosols are transported to eastern China from Asian inner continent (Zhou et al., 2018), and clay mineral is the major component of these dusts. Thus, with such an abundance of clay mineral, mixing particle formation from clay mineral with SA-amine is expected to be new potential source to aerosols during dust storm in megacities of China.

4. Conclusions

The mixing particle forming mechanism from amines with clay mineral are systematically investigated using combined theoretical and experimental methods. Mixing particle formation starting from water uptake is found to be competitive with SA uptake even at extreme dry condition. Subsequently, clay mineral surface is protonated by SA with or without water participation, and the generated clusters of Kao-SA and Kao-H₂O-SA act as key intermediates to further react with amines. Afterwards amines exist as molecule or converts into ammonium salt contained in final mixing particle, which is determined by the occurrence of water content and hydrogen bonding site type of protonated clay mineral surface. Furthermore, ammonium salt contributing to mixing particle mass is more efficiently promoted with the increased RH. Particularly for MA, water content is requirement for ammonium salt conversion during mixing particle formation, whereas it is not for DMA nor TMA. However, for TMA, mixing particle formation without water is more competitive than that with water, and more hydrophobic groups of -CH₃ in TMA account for this. Overall, our work confirmed mixing particle formation from amine with clay mineral is expected to

be new potential source to aerosols during dust storm. It is noteworthy that ammonium salts are supposed to be predominant components in mixing particle formed through the supposed mechanism in this work. Ammonium salt determines particle's hygroscopicity (Kim et al., 2016), and further affects the CCN/IN activity of particle (Wang et al., 2019). Therefore, the hygroscopicity growth of mixing particle and its influence on regional climate deserves further investigations.

CRediT authorship contribution statement

Weina Zhang: Conceptualization, Investigation, Methodology, Formal analysis and original draft. **Zhenhao Guo:** Methodology. **Weiping Zhang:** Methodology. **Yuemeng Ji:** Methodology. **Guiying Li:** Review & editing. **Taicheng An:** Review & editing, Supervision, Project administration, Funding acquisition.

Declaration of competing interest

The authors declare that they have no known competing financial interests or personal relationships that could have appeared to influence the work reported in this paper.

Acknowledgements

This work was financially supported by NSFC (42020104001, 41907184 and 42007327), Basic and applied basic research fund project of Guangdong Province (2021A1515011252), Local Innovative and Research Team Project of Guangdong Pearl River Talents Program (2017BT01Z032).

Appendix A. Supplementary data

Supplementary data to this article can be found online at <https://doi.org/10.1016/j.scitotenv.2022.153336>.

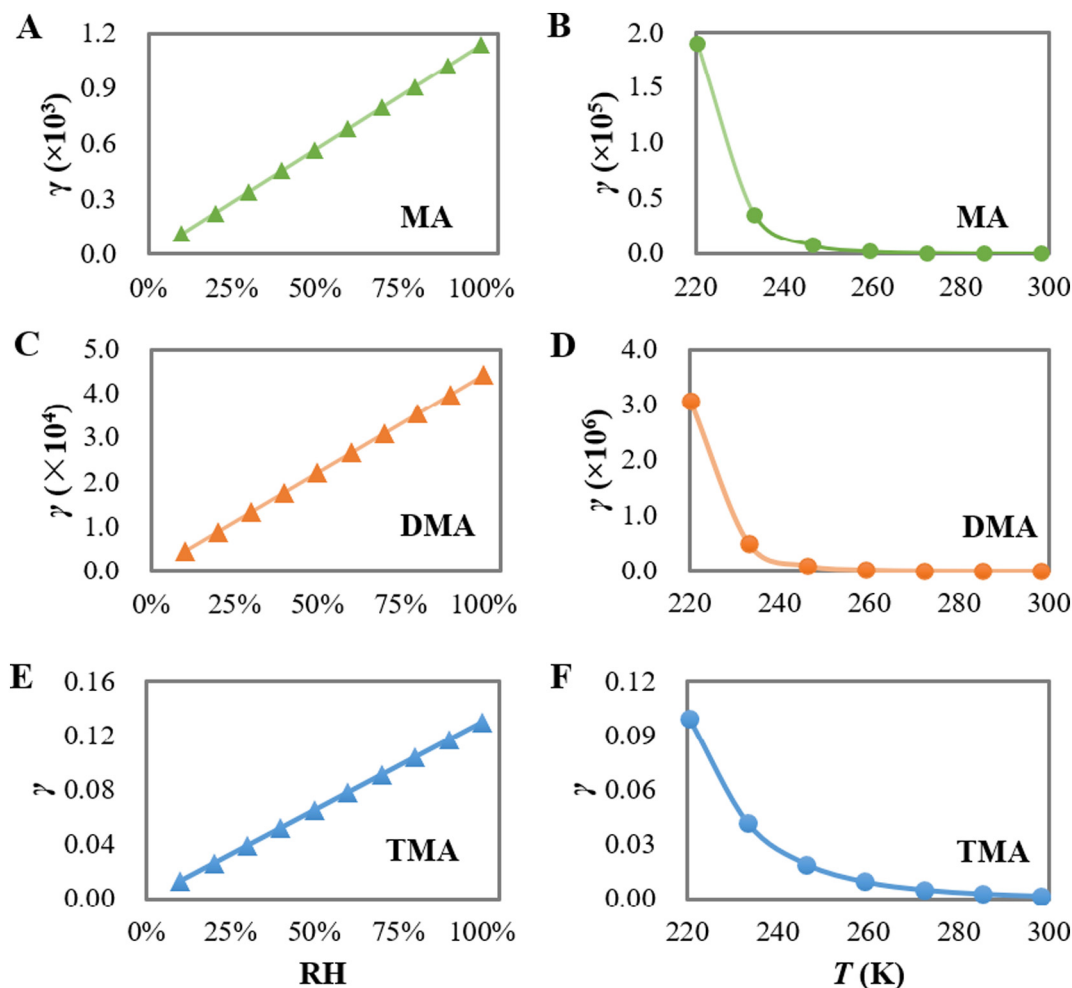


Fig. 6. γ profiles for (A, B) MA, (C, D) DMA and (E, F) TMA cases with increased RH and temperatures (T), respectively.

References

- Almeida, J., Schobesberger, S., Kurten, A., Ortega, I.K., Kupiainen-Maatta, O., Praplan, A.P., et al., 2013. Molecular understanding of sulphuric acid-amine particle nucleation in the atmosphere. *Nature* 502, 359–363.
- Burgos, M.A., Mateos, D., Cachorro, V.E., Toledano, C., de Frutos, A.M., 2016. Aerosol properties of mineral dust and its mixtures in a regional background of north-Central Iberian Peninsula. *Sci. Total Environ.* 572, 1005–1019.
- Chen, Y., Tong, S., Li, W., Liu, Y., Tan, F., Ge, M., et al., 2021. Photocatalytic oxidation of SO₂ by TiO₂: aerosol formation and the key role of gaseous reactive oxygen species. *Environ. Sci. Technol.* 55, 9784–9793.
- Cheng, C., Huang, Z., Chan, C.K., Chu, Y., Li, M., Zhang, T., et al., 2018. Characteristics and mixing state of amine-containing particles at a rural site in the Pearl River Delta, China. *Atmos. Chem. Phys.* 18, 9147–9159.
- Cuadros, J., Diaz-Hernandez, J.L., Sanchez-Navas, A., Garcia-Casco, A., 2015. Role of clay minerals in the formation of atmospheric aggregates of saharan dust. *Atmos. Environ.* 120, 160–172.
- Dawson, M.L., Varner, M.E., Perraud, V., Ezell, M.J., Gerber, R.B., Finlayson-Pitts, B.J., 2012. Simplified mechanism for new particle formation from methanesulfonic acid, amines, and water via experiments and ab initio calculations. *Proc. Natl. Acad. Sci. U. S. A.* 109, 18719–18724.
- DeMott, P.J., Prenni, A.J., Liu, X., Kreidenweis, S.M., Petters, M.D., Twohy, C.H., et al., 2010. Predicting global atmospheric ice nuclei distributions and their impacts on climate. *Proc. Natl. Acad. Sci. U. S. A.* 107, 11217–11222.
- Du, C., Kong, L., Zhazakova, A., Tong, S., Yang, X., Wang, L., et al., 2019. Impact of adsorbed nitrate on the heterogeneous conversion of SO₂ on alpha-Fe₂O₃ in the absence and presence of simulated solar irradiation. *Sci. Total Environ.* 649, 1393–1402.
- Erupe, M.E., Benson, D.R., Li, J., Young, L.-H., Verheggen, B., Al-Refai, M., et al., 2010. Correlation of aerosol nucleation rate with sulfuric acid and ammonia in Kent, Ohio: an atmospheric observation. *J. Geophys. Res.-Atmos.* 115, D23216.
- Ge, X., Wexler, A.S., Clegg, S.L., 2011. Atmospheric amines – Part I. A review. *Atmos. Environ.* 45, 524–546.
- Gong, H., Cheng, C., Li, M., Yang, S., Zhou, Q., Zhong, Q.E., et al., 2021. The enhanced mixing states of oxalate with metals in single particles in Guangzhou, China. *Sci. Total Environ.* 783.
- Gustafsson, R.J., Orlov, A., Badger, C.L., Griffiths, P.T., Cox, R.A., Lambert, R.M., 2005. A comprehensive evaluation of water uptake on atmospherically relevant mineral surfaces: DRIFT spectroscopy, thermogravimetric analysis and aerosol growth measurements. *Atmos. Chem. Phys.* 5, 3415–3421.
- Herich, H., Tritscher, T., Wiacek, A., Gysel, M., Weingartner, E., Lohmann, U., et al., 2009. Water uptake of clay and desert dust aerosol particles at sub- and supersaturated water vapor conditions. *Phys. Chem. Chem. Phys.* 11, 7804–7809.
- Ji, Y., Wang, H., Li, G., An, T., 2015. Theoretical investigation on the role of mineral dust aerosol in atmospheric reaction: a case of the heterogeneous reaction of formaldehyde with NO₂ onto SiO₂ dust surface. *Atmos. Environ.* 103, 207–214.
- Julin, J., Murphy, B.N., Patoulias, D., Fountoukis, C., Olenius, T., Pandis, S.N., et al., 2018. Impacts of future European emission reductions on aerosol particle number concentrations accounting for effects of ammonia, amines, and organic species. *Environ. Sci. Technol.* 52, 692–7000.
- Kadar, E., Cunliffe, M., Fisher, A., Stolpe, B., Lead, J., Shi, Z., 2014. Chemical interaction of atmospheric mineral dust-derived nanoparticles with natural seawater - EPS and sunlight-mediated changes. *Sci. Total Environ.* 468, 265–271.
- Kim, J., Ahlm, L., Yli-Juuti, T., Lawler, M., Keskinen, H., Troestl, J., et al., 2016. Hygroscopicity of nanoparticles produced from homogeneous nucleation in the CLOUD experiments. *Atmos. Chem. Phys.* 16, 293–304.
- Kok, J.F., Ridley, D.A., Zhou, Q., Miller, R.L., Zhao, C., Heald, C.L., et al., 2017. Smaller desert dust cooling effect estimated from analysis of dust size and abundance. *Nat. Geosci.* 10, 274–278.
- Kresse, G., Furthmüller, J., 1996. Efficiency of ab-initio total energy calculations for metals and semiconductors using a plane-wave basis set. *Comput. Mater. Sci.* 6, 15–50.
- Kumar, S., Rosenberg, J.M., Bouzida, D., Swendsen, R.H., Kollman, P., 1995. Multidimensional free-energy calculations using the weighted histogram analysis method. *J. Comput. Chem.* 16, 1339–1350.
- Li, Y., Ji, Y., Zhao, J., Wang, Y., Shi, Q., Peng, J., et al., 2021. Unexpected oligomerization of small α -dicarbonyls for secondary organic aerosol and Brown carbon formation. *Environ. Sci. Technol.* 55, 4430–4439.
- Liu, Y., Ma, Q., He, H., 2012. Heterogeneous uptake of amines by citric acid and humic acid. *Environ. Sci. Technol.* 46, 11112–11118.
- Lv, S.-S., Miao, S.-K., Ma, Y., Zhang, M.-M., Wen, Y., Wang, C.-Y., et al., 2015. Properties and atmospheric implication of methylamine sulfuric acid-water clusters. *J. Phys. Chem. A* 119, 8657–8666.

- Moteki, N., Adachi, K., Ohata, S., Yoshida, A., Harigaya, T., Koike, M., 2017. Anthropogenic iron oxide aerosols enhance atmospheric heating. *Nat. Commun.* 8.
- Nadykto, A.B., Herb, J., Yu, F., Xu, Y., 2014. Enhancement in the production of nucleating clusters due to dimethylamine and large uncertainties in the thermochemistry of amine-enhanced nucleation. *Chem. Phys. Lett.* 609, 42–49.
- Olenius, T., Kupiainen-Maatta, O., Ortega, I.K., Kurten, T., Vehkamäki, H., 2013. Free energy barrier in the growth of sulfuric acid-ammonia and sulfuric acid-dimethylamine clusters. *J. Chem. Phys.* 139, 084312.
- Olenius, T., Halonen, R., Kurten, T., Henschel, H., Kupiainen-Maatta, O., Ortega, I.K., et al., 2017. New particle formation from sulfuric acid and amines: comparison of monomethylamine, dimethylamine, and trimethylamine. *J. Geophys. Res. Atmos.* 122, 7103–7118.
- Phillips, J.C., Braun, R., Wang, W., Gumbart, J., Tajkhorshid, E., Villa, E., et al., 2005. Scalable molecular dynamics with NAMD. *J. Comput. Chem.* 26, 1781–1802.
- Ponczek, M., George, C., 2018. Kinetics and product formation during the photooxidation of butanol on atmospheric mineral dust. *Environ. Sci. Technol.* 52, 5191–5198.
- Ryder, O.S., Ault, A.P., Cahill, J.F., Guasco, T.L., Riedel, T.P., Cuadra-Rodriguez, L.A., et al., 2014. On the role of particle inorganic mixing state in the reactive uptake of N₂O₅ to ambient aerosol particles. *Environ. Sci. Technol.* 48, 1618–1627.
- Shen, J., Elm, J., Xie, H.-B., Chen, J., Niu, J., Vehkamäki, H., 2020. Structural effects of amines in enhancing methanesulfonic acid-driven new particle formation. *Environ. Sci. Technol.* 54, 13498–13508.
- Sipila, M., Berndt, T., Petaja, T., Brus, D., Vanhanen, J., Stratmann, F., et al., 2010. The role of sulfuric acid in atmospheric nucleation. *Science* 327, 1243–1246.
- Song, C.H., Nam, J.E., Han, K.M., Lee, M.K., Woo, J.H., Han, J.S., 2012. Influence of mineral dust mixing-state and reaction probabilities on size-resolved sulfate formation in Northeast Asia. *Atmos. Environ.* 58, 23–34.
- Tan, F., Jing, B., Tong, S., Ge, M., 2017. The effects of coexisting Na₂SO₄ on heterogeneous uptake of NO₂ on CaCO₃ particles at various RHs. *Sci. Total Environ.* 586, 930–938.
- Tenney, C.M., Cygan, R.T., 2014. Molecular simulation of carbon dioxide, brine, and clay mineral interactions and determination of contact angles. *Environ. Sci. Technol.* 48, 2035–2042.
- Tian, P., Zhang, L., Ma, J., Tang, K., Xu, L., Wang, Y., et al., 2018. Radiative absorption enhancement of dust mixed with anthropogenic pollution over East Asia. *Atmos. Chem. Phys.* 18, 7815–7825.
- Tong, D., Chen, J., Qin, D., Ji, Y., Li, G., An, T., 2020. Mechanism of atmospheric organic amines reacted with ozone and implications for the formation of secondary organic aerosols. *Sci. Total Environ.* 737.
- VandenBoer, T.C., Petroff, A., Markovic, M.Z., Murphy, J.G., 2011. Size distribution of alkyl amines in continental particulate matter and their online detection in the gas and particle phase. *Atmos. Chem. Phys.* 11, 4319–4332.
- Wang, Z., Pan, X., Uno, I., Chen, X., Yamamoto, S., Zheng, H., et al., 2018. Importance of mineral dust and anthropogenic pollutants mixing during a long-lasting high PM event over East Asia. *Environ. Pollut.* 234, 368–378.
- Wang, Z., Wang, T., Fu, H., Zhang, L., Tang, M., George, C., et al., 2019. Enhanced heterogeneous uptake of sulfur dioxide on mineral particles through modification of iron speciation during simulated cloud processing. *Atmos. Chem. Phys.* 19, 12569–12585.
- Xie, H.-B., Elm, J., Halonen, R., Myllys, N., Kurten, T., Kulmala, M., et al., 2017. Atmospheric fate of monoethanolamine: enhancing new particle formation of sulfuric acid as an important removal process. *Environ. Sci. Technol.* 51, 8422–8431.
- Yang, W., Ma, Q., Liu, Y., Ma, J., Chu, B., He, H., 2019. The effect of water on the heterogeneous reactions of SO₂ and NH₃ on the surfaces of alpha-Fe₂O₃ and gamma-Al₂O₃. *Environ. Sci. Nano* 6, 2749–2758.
- Yang, N., Tsona, N.T., Cheng, S., Wang, Y., Wu, L., Ge, M., et al., 2020. Effects of NO₂ and SO₂ on the heterogeneous reaction of acetic acid on alpha-Al₂O₃ in the presence and absence of simulated irradiation. *Environ. Sci. Process Impacts* 22, 408–417.
- Yao, L., Garmash, O., Bianchi, F., Zheng, J., Yan, C., Kontkanen, J., et al., 2018. Atmospheric new particle formation from sulfuric acid and amines in a Chinese megacity. *Science* 361, 278–281.
- Yin, R., Yan, C., Cai, R., Li, X., Shen, J., Lu, Y., et al., 2021. Acid-Base clusters during atmospheric new particle formation in urban Beijing. *Environ. Sci. Technol.* 55, 10994–11005.
- Yu, Z., Jang, M., 2018. Simulation of heterogeneous photooxidation of SO₂ and NO_x in the presence of Gobi Desert dust particles under ambient sunlight. *Atmos. Chem. Phys.* 18, 14609–14622.
- Zhang, R.Y., Suh, I., Zhao, J., Zhang, D., Fortner, E.C., Tie, X.X., et al., 2004. Atmospheric new particle formation enhanced by organic acids. *Science* 304, 1487–1490.
- Zhang, W., Ji, Y., Li, G., Shi, Q., An, T., 2019. The heterogeneous reaction of dimethylamine/ammonia with sulfuric acid to promote the growth of atmospheric nanoparticles. *Environ. Sci. Nano* 6, 2767–2776.
- Zhang, Y., Gao, T., Kang, S., Sprenger, M., Tao, S., Du, W., et al., 2020. Effects of black carbon and mineral dust on glacial melting on the Muztagh glacier, Central Asia. *Sci. Total Environ.* 740, 140056.
- Zhang, W., Zhong, J., Shi, Q., Gao, L., Ji, Y., Li, G., et al., 2021. Mechanism for rapid conversion of amines to ammonium salts at the air-particle interface. *J. Am. Chem. Soc.* 143, 1171–1178.
- Zhou, D., Ding, K., Huang, X., Liu, L., Liu, Q., Xu, Z., et al., 2018. Transport, mixing and feedback of dust, biomass burning and anthropogenic pollutants in eastern Asia: a case study. *Atmos. Chem. Phys.* 18, 16345–16361.